over the continental United States during the spring and winter seasons (not shown) suggests that the impact of the land is primarily a contemporaneous feedback and not the result of memory of the previous season's anomalies. We note that the observations do show substantial precipitation deficits to the north and east of the core region during spring, but similar anomalies are also obtained for some of the individual model runs, suggesting that the observed precipitation anomalies in the spring may not have been forced by SST anomalies.

25. C. A. Woodhouse, J. T. Overpeck, *Bull. Am. Meteorol. Soc.* **79**, 2693 (1998).
26. D. L. Bark, in *North American Droughts*, N. J. Rosenberg, Ed. (AAAS Selected Symposia Series, Westview Press, Boulder Colorado, 1978), pp. 9–23.
27. U.S. Drought Monitoring Page (www.drought.unl.edu/dm/monitor.html).
28. Y. Zhang, J. M. Wallace, D. Battisti, *J. Clim.* **10**, 1004 (1997).
29. This work was supported by the NASA Earth Science

Laboratory Earthquakes: The Sub-Rayleigh–to–Supershear Rupture Transition

Kaiwen Xia,[1,2] Ares J. Rosakis,[2] Hiroo Kanamori[1]*

We report on the experimental observation of spontaneously nucleated supershear rupture and on the visualization of sub-Rayleigh–to–supershear rupture transitions in frictionally held interfaces. The laboratory experiments mimic natural earthquakes. The results suggest that under certain conditions supershear rupture propagation can be facilitated during large earthquake events.

The surface-wave magnitude (M_s) 8.1 (M_w 7.8) central Kunlunshan earthquake that occurred on 14 November 2001 was an extraordinary event from the point of view of dynamic rupture mechanics. The rupture occurred over a long, near-vertical, strike-slip fault segment of the active Kunlunshan fault and featured an exceptionally long (400 km) surface rupture zone and large surface slip displacements (*1*). Modeling of the rupture speed history (*2*) suggests rupture speeds that are slower than the Rayleigh wave speed, c_R, for the first 100 km, transitioning to supershear (speed higher than the shear wave speed, c_S) for the remaining 300 km of rupture growth. Other events, such as the 1979 Imperial Valley earthquake (*3, 4*), the 1992 Landers earthquake (*5*), the 1999 Izmit earthquake (*6*), and the 2002 Denali earthquake (*7*), may also have featured supershear speeds. Supershear was also predicted theoretically (*8, 9*) and numerically (*10, 11*). Even with these estimates and predictions at hand, the question of whether natural earthquake ruptures can propagate at supershear speeds is still a subject of active debate. In addition, the exact mechanism for transition of a spontaneously nucleated rupture from sub-Rayleigh to supershear rupture speed is not clear. One answer to this question was provided by the two-dimensional Burridge-

Andrews mechanism (BAM) (*10*). Recent numerical investigations of frictional rupture have suggested alternative, asperity-based, three-dimensional mechanisms (*12–14*). Whether and how supershear rupture occurs during earthquakes has important implications for seismic hazards, because the rupture speed influences the character of near-field ground motions.

To answer the above-stated questions, we conducted experiments that mimic the earthquake rupture processes. Our goal was to examine the physical plausibility and conditions under which supershear ruptures can be generated in a controlled laboratory environment. We studied spontaneously nucleated dynamic rupture events in incoherent, frictional interfaces held together by far-field tectonic loads. Thus, we departed from experimental work that addresses the supershear ruptures of coherent interfaces loaded by impact-induced stress waves (*15, 16*).

An exploding wire-triggering mechanism (Fig. 1C), which simulates a localized pressure release, was used to trigger the rupture (*17*). This triggering mechanism is inspired by recent numerical work on rupture along frictional interfaces (*18, 19*). Experimentally, it is a convenient way of triggering the system's full-field, high-speed diagnostics (Fig. 1A) that would otherwise be unable to capture an event with a total duration of ~50 μs.

More than 50 experiments, featuring a range of angles α and far-field pressures P, were performed, and the symmetric bilateral rupture process histories were visualized in intervals of 2 μs. Depending on P and α, rupture speeds that are either sub-Rayleigh or

supershear were observed. The maximum shear stress field for an experiment with α = 25° and P = 7 MPa (Fig. 2A) shows that the speed of the rupture tip is very close to c_R and follows closely behind the circular shear wave front that is emitted at the time of rupture nucleation. The same was found to be true for smaller angles and lower pressures. For an experiment with α = 25° and P = 15 MPa (Fig. 2B), the circular trace of the shear wave is also visible and is at the same location as in Fig. 2A. However, in front of this circle a supershear disturbance, featuring a Mach cone (pair of shear shock waves), is clearly visible. For this case, the sequences of images before 28 μs have a similar form to the image displayed in Fig. 2B and reveal a disturbance that was nucleated as supershear. Its speed history, $v(t)$, is determined independently by either the rupture length record or by measuring the angle, β, of the shear shocks with respect to the fault plane and with the use of the relation $v = c_S/\sin β$. Its speed was 1970 m/s, which is close to the longitudinal wave speed c_P. In previous experiments involving strong, coherent interfaces and stress wave loading, stable rupture speeds near $\sqrt{2}c_S$ were observed (*15*). This apparent discrepancy can be explained by referring to the rupture velocity dependence on the available energy per unit crack advance within the supershear regime (*16*). This energy attains a maximum value at speeds closer to $\sqrt{2}c_S$ for strong interfaces. For weaker interfaces, this maximum moves toward c_P.
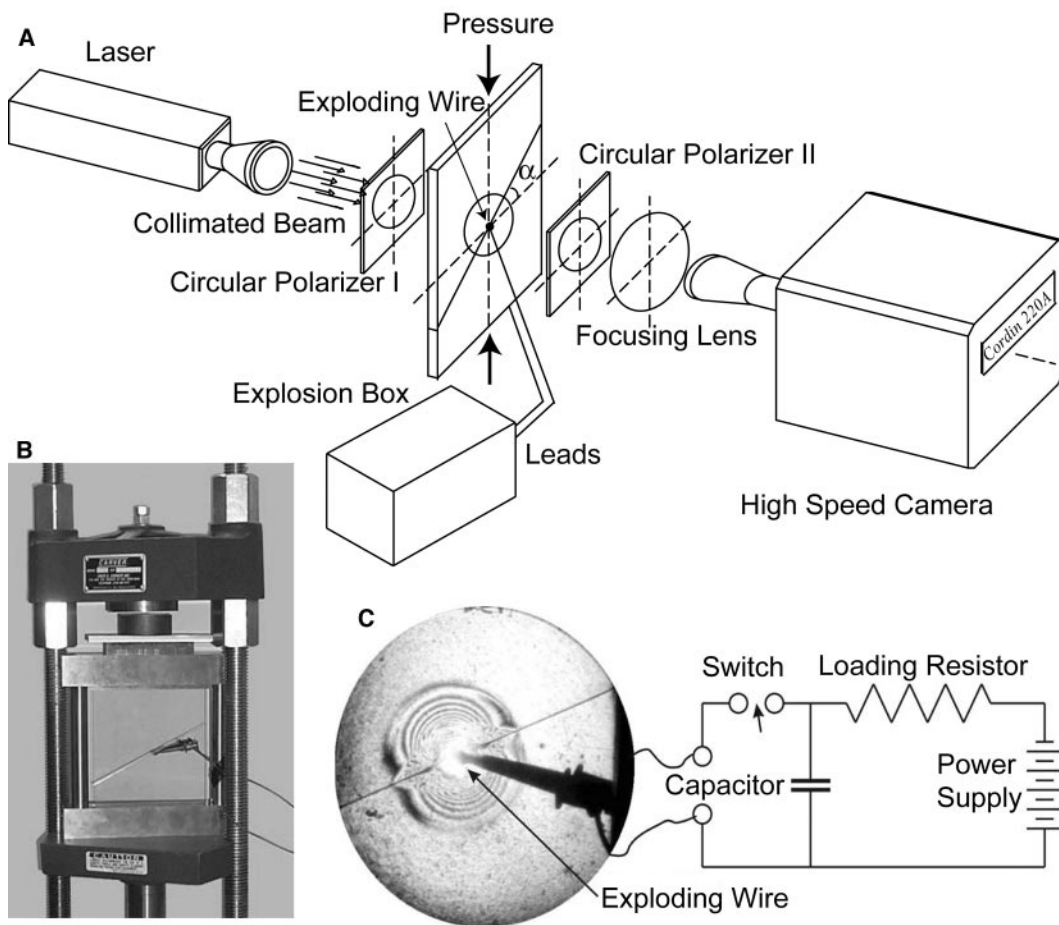
To visualize a transition within our field of view (100 mm), we kept α = 25° but reduced P to 9 MPa (Fig. 3, A to C). The circular traces of P and S waves are visible, followed by a rupture propagating initially at c_R (Fig. 3A). A small secondary rupture appears in front of the main rupture and propagates slightly ahead of the S wave front (Fig. 3B). The two ruptures coalesce, and the leading edge of the resulting rupture grows at a speed close to c_P. The transition length L here is ~20 mm (Fig. 3D).

The above transition phenomenon is comparable with BAM, which is described in (*20*). Andrews investigated this transition in a parameter space spanned by a normalized supershear transition length, L/L_c, and a non-dimensional driving stress parameter, s [s =

[1]Seismological Laboratory, MC 252-21, California Institute of Technology (Caltech), Pasadena, CA 91125, USA. [2]Graduate Aeronautical Laboratories, MC 105-50, Caltech, Pasadena, CA 91125, USA.

*To whom correspondence should be addressed. E-mail: hiroo@gps.caltech.edu

Fig. 1. The diagnostics is photoelasticity combined with high-speed photography (up to 10^8 frames/s). The fault system is simulated by using two photoelastic plates (homalite-100, shear modulus $G = 1.4$ GPa, Poisson's ration = 0.35, density $\rho = 1200$ kg/m^3) held together by friction. The interface (fault) is inclined at an angle α to the horizontal promoting strike-slip rupture events (**A**). The carefully prepared interface has a measured static coefficient of friction $\mu^s = 0.6$; the dynamic coefficient of friction μ^d is estimated by finding the critical α of triggered events, which is between 10° and 15°, and hence $\mu^d = 0.2$ is estimated. The far-field tectonic loading is simulated by uniaxial compression exerted at the top and bottom ends of the system by a hydraulic press (**B**). The dynamic rupture is nucleated at the center of the simulated fault by producing a local pressure pulse in a small area of the interface (*17*). A thin wire of 0.1 mm in diameter is inserted in a small hole of the same size. An electronic condenser is then discharged, turning the metal into expanding plasma to provide the controllable pressure pulse (**C**).

$(\tau^y - \tau)/(\tau - \tau^f)]$. The parameters τ, τ^y, and τ^f are the resolved shear stress on the fault and the static and the dynamic strength of the fault, respectively, which describe the linear slip-weakening frictional law (*21*). In our experiment, s can be expressed as $s = (\mu^s\cos\alpha - \sin\alpha)/(\sin\alpha - \mu^d\cos\alpha)$, where μ^s and μ^d are the static and dynamic coefficients of friction, respectively. Andrews' result can be written as $L = L_c f(s)$. The function $f(s)$ has been given numerically and can be approximated by $f(s) = 9.8(1.77 - s)^{-3}$. The normalizing length, L_c, is the critical length for unstable rupture nucleation and is proportional to the rigidity, G, and to d_0, which is the critical or breakdown slip of the slip-weakening model. L can then be expressed as

$$L = f(s)[(1 + v)/\pi][(\tau^y - \tau^f)/$$
$$(\tau - \tau^f)^2]Gd_0 \qquad (1)$$

Applying Eq. 1 to our experiments, the transition length is inversely proportional to the applied uniaxial pressure, P, as

$$L = f(s)[(1 + v)/\pi]G[(\mu^s - \mu^d)/$$
$$(\tan\alpha - \mu^d)^2](d_0/P) \qquad (2)$$

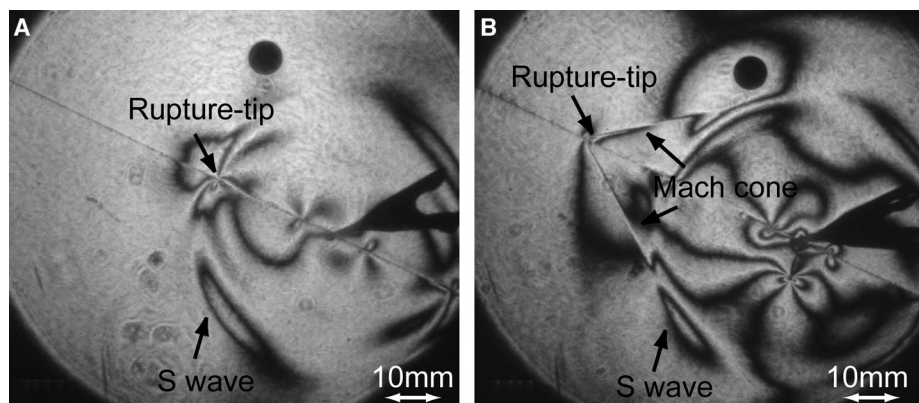We can compare our experiments to Andrews' theory (Fig. 4). Although the theory

Fig. 2. Purely sub-Rayleigh ($\alpha = 25°$ and $P = 7$ MPa) (**A**) and purely supershear ($\alpha = 25°$ and $P = 15$ MPa (**B**) rupture at the same time (28 μs) after triggering.

qualitatively captures the trends of the experiments, the data exhibit a dependence on pressure stronger than P^{-1}.

A natural way to modify Andrews' results is to introduce some microcontact physics and to thus consider the effect of pressure on d_0. We first note that there exists a linear relation between a characteristic surface length (half-distance between contacting asperities, D) and the critical slip distance d_0 $\{d_0 = c[(\tau^y - \tau^f)/\tau^f]^M D$, where c and M are constants$\}$ (*22*). We then denote the normal stress applied on the fault as σ ($\sigma = P\cos^2\alpha$)

and assume that the average radius of n contacting asperities, a_0, is constant. As the pressure over a macroscopic contact area, A (equal to $n\pi D^2$), is increased, n, as well as the real contact area, A_r (equal to $n\pi a_0^2$), increase. By defining the hardness, H, as the ratio of the normal force N to A_r (*23*), N can be expressed as $N = HA_r = \sigma A = AP\cos^2\alpha$. Substitution of A and A_r in terms of D and a_0, respectively, gives $D = \sqrt{H}\, a_0\cos\alpha P^{-1/2}$. With the use of the relation $d_0 \propto D$, d_0 is found to depend on the pressure as $d_0 \propto P^{-1/2}$. By further using Eq. 2, a modified expression
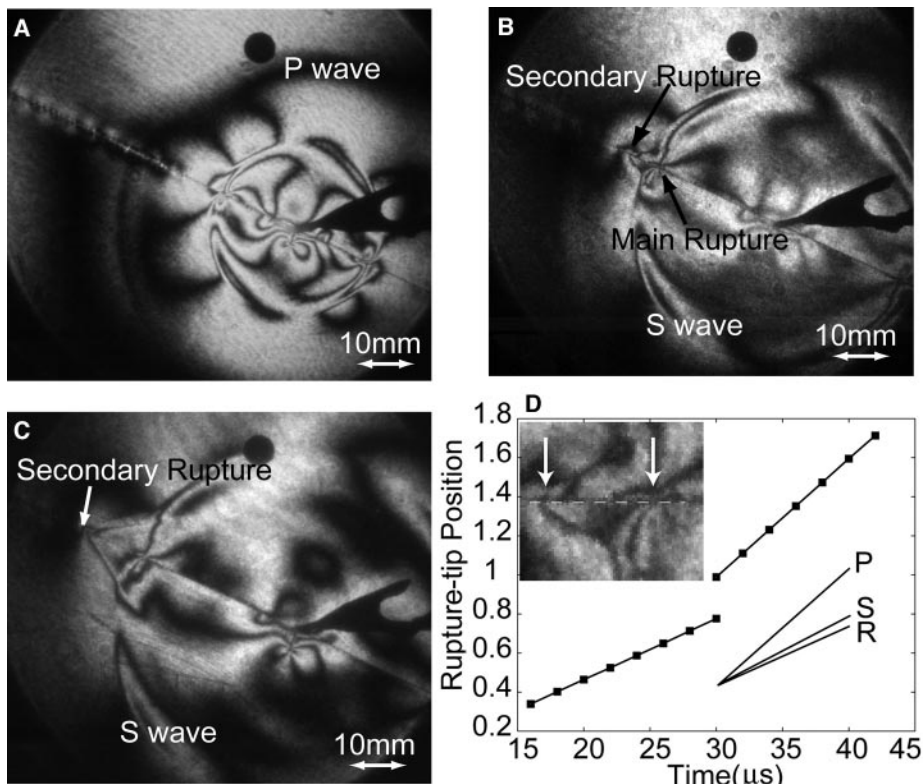
Fig. 3. Visualization of the sub-Rayleigh–to–supershear rupture transition ($\alpha = 25°$ and $P = 9$ MPa). (**A** to **C**) were taken at 18 μs, 30 μs, and 38 μs, respectively. In the rupture-tip history plot (**D**), we included lines corresponding to P, S, and Rayleigh waves as reference.
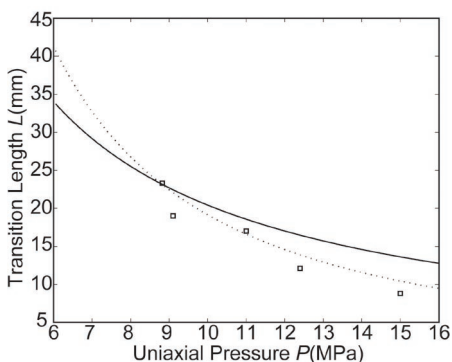

Fig. 4. Transition length as a function of far-field load. Solid curve is Andrew's theory, dashed curve is modified theory, and squares are experimental data.

relating L to P emerges, featuring a stronger pressure dependence ($L \propto P^{-3/2}$). This modified relation, which agrees well with the experimental data (Fig. 4), is given by

$$L = f(s)\frac{1 + \nu}{\pi}\,G\,\frac{\mu^s - \mu^d}{[\sin\alpha - \mu^d\cos\alpha]^2}$$
$$2c\left(\frac{\mu^s - \mu^d}{\mu^s}\right)\sqrt{H}a_0 P^{-\frac{3}{2}}\cos^{-1}\alpha \quad (3)$$

For seismic applications, we rewrite Eq. 1 in terms of the effective stress, $\tau_e = \tau - \tau^f$, as $L = f(s)(1 + \nu)(1 + s)Gd_0/\pi\tau_e$. Application of this equation to both seismic faulting and to laboratory data allows us to scale L from laboratory to seismological conditions. The stress τ_e in our experiments is chosen to be of the same order as that in seismology. The ratio of rigidity of the Earth's crust to homalite is 25. We estimate $L = 20$ mm from the experiment where $P = 9$ MPa, $\alpha = 25°$, and $d_0 = 10$ μm (obtained with the use of Eq. 2). The values of d_0 for large earthquakes are often estimated as 50 cm to 1 m (24). Thus, if s is about the same under laboratory and crustal conditions, L for earthquakes can be estimated to be in the range between 25 and 50 km. Because s can be different and the estimate of d_0 for earthquakes is uncertain, this value should be taken as an order-of-magnitude estimate. Nevertheless, it is of the same order as that inferred for the Kunlunshan event (2).

The large L required for supershear is one of the reasons why only a few earthquake events have been observed to feature supershear speeds. It suggests that in such cases the tectonic stress is fairly close to the static fault strength (i.e., small s), which has important implications for evolution of rupture in large earthquakes.

References and Notes

1. A. Lin *et al.*, *Science* **296**, 2015 (2002).
2. M. Bouchon, M. Vallee, *Science* **301**, 824 (2003).
3. R. J. Archuleta, *J. Geophys. Res.* **89**, 4559 (1984).
4. P. Spudich, E. Cranswick, *Bull. Seismol. Soc. Am.* **74**, 2083 (1984).
5. K. B. Olsen, R. Madariaga, R. J. Archuleta, *Science* **278**, 834 (1997).
6. M. Bouchon *et al.*, *Geophys. Res. Lett.* **28**, 2723 (2001).
7. W. L. Ellsworth *et al.*, paper presented at the Eleventh International Conference on Soil Dynamics and Earthquake Engineering, Berkeley, CA, 7 to 9 January 2004.
8. R. Burridge, *Geophys. J. R. Astron. Soc.* **35**, 439 (1973).
9. R. Burridge, G. Conn, L. B. Freund, *J. Geophys. Res.* **84**, 2210 (1979).
10. D. J. Andrews, *J. Geophys. Res.* **81**, 5679 (1976).
11. S. Das, K. Aki, *Geophys. J. R. Astron. Soc.* **50**, 643 (1977).
12. S. M. Day, *Bull. Seismol. Soc. Am.* **72**, 1881 (1982).
13. R. Madariaga, K. B. Olsen, *Pure Appl. Geophys.* **157**, 1981 (2000).
14. E. M. Dunham, P. Favreau, J. M. Carlson, *Science* **299**, 1557 (2003).
15. A. J. Rosakis, O. Samudrala, D. Coker, *Science* **284**, 1337 (1999).
16. A. J. Rosakis, *Adv. Phys.* **51**, 1189 (2002).
17. Before the triggering of the discharge, the fault system is in equilibrium because the resolved shear traction along the fault is balanced by the static friction strength. After triggering, the expansion of the high-pressure plasma at the simulated hypocenter creates a pressure pulse that releases the local normal pressure of the interface, thus dropping the level of frictional resistance. The resultant net driving force then initiates bilateral slip along the fault. The slip and slip rate reduce the coefficient of friction (slip and/or slip rate weakening) and hence, for a large enough inclination angle α, the rupture is able to continue. Thus, simulated earthquakes are triggered in the laboratory.
18. D. J. Andrews, Y. BenZion, *J. Geophys. Res.* **102**, 553 (1997).
19. A. Cochard, J. R. Rice, *J. Geophys. Res.* **105**, 25891 (2000).
20. Classical dynamic fracture theories of growing shear cracks have many similarities to the earthquake rupture processes (25, 26). Such theories treat the rupture front as a distinct point (sharp tip crack) of stress singularity. Such conditions are closer to reality in cases that feature coherent interfaces of finite intrinsic strength and toughness. The singular approach ultimately predicts that dynamic shear fracture cannot propagate in the small interval between c_R and c_S and thus excludes the possibility of a smooth transition from sub-Rayleigh to supershear. The introduction of a distributed rupture process zone has allowed fracture mechanics to better approximate the conditions that exist during real earthquake events (21) and to describe mechanisms for a sub-Rayleigh rupture to enter the supershear regime. According to the two-dimensional BAM, a shear rupture accelerates to a speed very close to c_R soon after its initiation. A peak in shear stress is found to propagate at the shear wave front and is observed to increase its magnitude as the main rupture speed approaches c_R. At that point, the shear stress peak may become strong enough to promote the nucleation of a secondary microrupture whose leading edge propagates at c_P. Shortly thereafter, the two ruptures join up, and the combination propagates at c_P. This transition was visualized by two-dimensional atomistic calculations of shear rupture in the microscale (27).
21. A. C. Palmer, J. R. Rice, *Proc. R. Soc. London Ser. A* **332**, 527 (1973).
22. M. Ohnaka, *J. Geophys. Res.* **108**, 10.1029/2000JB000123 (2003).
23. F. P. Bowden, D. Tabor, *The Friction and Lubrication of Solids* (Clarendon Press, Oxford, 1986), p. 374.
24. S. Ide, M. Takeo, *J. Geophys. Res.* **102**, 27379 (1997).
25. L. B. Freund, *Dynamic Fracture Mechanics* (Cambridge Univ. Press, Cambridge, 1990), p. 563.
26. K. B. Broberg, *Cracks and Fracture* (Academic Press, San Diego, CA, 1999), p. 752.
27. F. F. Abraham, H. J. Gao, *Phys. Rev. Lett.* **84**, 3113 (2000).
28. Authors appreciate fruitful discussions with T. Heaton and G. Ravichandran from Caltech and J. R. Rice from Harvard. This study is supported by NSF grant EAR-0207873 and Office of Naval Research grant N00014-03-1-0435.